Supporting Information for:

Synthesis, Characterization, and Nitrogenase-Relevant Reactions of an Iron Sulfide Complex with a Bridging Hydride

*Nicholas A. Arnet, Thomas R. Dugan, Fabian S. Menges, Brandon Q. Mercado, William W. Brennessel, Eckhard Bill, Mark A. Johnson, and Patrick L. Holland**

* email: patrick.holland@yale.edu

Table of Contents

General Considerations. Unless otherwise noted, all reactions were performed under an argon atmosphere in an M. Braun glovebox maintained at or below 1 ppm of O_2 and H_2O. Glassware was dried at 160 ˚C and Celite was dried at 200 ˚C under vacuum. Solvents were dried by passage through activated alumina and Q5 columns from Glass Contour Co., with the exception of THF, which was distilled under Ar from a potassium benzophenone ketyl solution. All solvents were stored over activated 4 Å molecular sieves. Benzene-d_6 was dried and stored over activated alumina and filtered before use. THF-d_8 was dried in a potassium benzophenone ketyl solution and distilled before used. Pyridine-d_5 was dried over 4 Å molecular sieves. The hydride complex $[L^{Me}FeH]_2$ and deuteride complex $[L^{Me}FeD]_2$ were prepared according to published procedures.[1] Sodium dodecanethiolate ($NaSC_{12}H_{25}$) was synthesized by adding sodium hydride (109.3 mg, 4.554 mmol), purchased from Acros Organics, to a solution of 1-dodecanethiol, purchased from the Sigma-Aldrich Corporation (10 mL of a 0.5 M solution in THF, 5 mmol). Lithium dodecanethiolate ($LiSC_{12}H_{25}$) was synthesized by adding *n*-butyllithium (1.50 mL of a 2.5 M solution in THF, 3.7 mmol), purchased from Acros Organics, to a solution of 1-dodecanethiol, purchased from Sigma-Aldrich Corporation, (636.7 mg, 3.417 mmol) dissolved in 5 mL THF. A magnetic stir bar was added and the reaction stirred loosely capped for 24 hours. The white solid was washed with THF and dried under vacuum, and used as a powder. Potassium graphite (KC_8) was prepared by heating stoichiometric amounts of potassium and graphite to 160 ˚C under an argon atmosphere. Lutidinium chloride was prepared by mixing lutidine (1.00 mL, 8.59 mmol) with 2.0 M HCl in diethylether (4.30 mL, 8.60 mmol) and washing the white solid product with diethyl ether. Sodium triphenylmethanethiolate was prepared dissolving triphenylmethanethiol (46.5 mg, 0.168 mmol) in THF (~3 mL) and adding sodium hydride (4.6 mg, 0.19 mmol). The product was isolated as a solid and washed with THF.

The 2.2.2-cryptand was purchased from Acros Organics. The 3-ethynyltoluene and triphenylmethanethiol was purchased from the Sigma-Aldrich Corporation. Carbon dioxide gas (research grade) was purchased from Airgas, Inc. Hydrogen gas (research grade) and methane gas (tech grade) were purchased from TechAir. D_2 (99.8%) and $^{13}CO_2$ (99%) were purchased from Cambridge Isotope Laboratories.

^{1}H NMR data were recorded on a Bruker Avance 500 spectrometer (500 MHz) or a Bruker Avance 400 spectrometer (400 MHz). All resonances in the ^{1}H NMR spectra are referenced to the residual solvent peaks (δ 7.16 ppm for benzene, δ 3.58 ppm for THF, δ 8.74 ppm for pyridine). Resonances were singlets unless otherwise noted. IR data were recorded on a Bruker ALPHA spectrometer equipped with a Platinum-ATR attachment. UV-vis spectra were recorded on a Cary 60 spectrophotometer using Schlenk-adapted quartz cuvettes with a 1 mm or 1 cm optical path length. Solution magnetic susceptibilities were determined by adding an internal capillary standard of the appropriate deuterated solvent to 2-7 mM ^{1}H NMR samples of metal complex. The difference between the capillary and solvent peaks in Hz was used to determine μ_{eff} via the Evans method, using at least two different concentrations for verification.[2] Mössbauer data were recorded on a SEECo spectrometer with alternating constant acceleration; isomer shifts are relative to iron metal at 298 K. The sample temperature was maintained at 80 K in a Janis Research Company Inc. cryostat. The zero-field spectra were simulated using Lorentzian doublets using WMoss (SeeCo). GC/MS analyses were performed on a Agilent GC 6890N and MS 5973 equipped with an RTX-1 column (15.0 m x 250 μm x 0.25 μm) using helium as the carrier gas. The analysis method used in all cases was 1.0 μL injection of sample, injection temperature of 250 ˚C, 100:1 split ratio, initial inlet pressure of 1.10 psi (but varied as the column flow was held constant at 1.0 mL/min for the duration of the run), the interface

temperature was held at 280 ˚C, and the ion source (EI, 70 eV) was held at 230 ˚C. The initial oven temperature was held at 50 ˚C for 3 min followed by a temperature ramp to 300 ˚C at 20 ˚C/min, and finally the temperature was held at 300 ˚C for 2 min. Elemental analyses were obtained from the CENTC Elemental Analysis Facility at the University of Rochester. Microanalysis samples were weighed with a PerkinElmer Model 2400 Series II Analyzer, and handled in a VAC Atmospheres glovebox under argon. Cyclic voltammetry data were recorded using a PINE WaveNow potentiostat inside N_2-filled glovebox. A Pt ceramic patterned electrode was used as the working and counter electrode. A silver electrode was used as a quasireference. The electrolyte was a 0.10 M solution of tetrabutylammonium hexafluorophosphate in dry THF. A scan rate of 50 mV/s was used. Potentials were referenced to the Cp_2Fe^+/Cp_2Fe couple using an internal ferrocene standard. Differential pulse voltammetry was collected using a pulse height of 75 mV, pulse width of 60 ms, period of 120 ms, and increments of 2 mV.

Headspace gas analyses were performed using a Thermo Scientific Trace 1300 gas chromatograph. Reactions were stirred under an N_2 atmosphere in 5 mL THF in a 25 mL round bottom flask sealed with a 180˚ vacuum adaptor capped with a rubber septum. At the beginning of the reaction, 400 μL of methane was injected into the headspace. After 1 hour, a 250 μL gas tight Hamilton syringe was used to draw 200 μL of headspace through the stopcock of the vacuum adaptor and injected into an SSL injection port. The samples ran through a mol sieve 5Å PLOT capillary GC column (30 m length, 0.53 mm inner diameter, 30 μm average thickness) purchased from Sigma-Aldrich at 0.95 mL/min flow of N_2 carrier gas and a constant oven temperature of 35 ˚C. Samples were detected using a TCD detector set to negative polarity. Samples were quantified using a calibration curve created by identical methods, injecting H_2 in quantities of 20, 40, 60, 80, and 100 μL into the headspace of the flask.

Electrospray Mass Spectra were recorded in a modified FT-ICR-MS instrument (Bruker Apex I) equipped with a 7.0 T magnet, an electrospray ion source (Analytica) and a NHMFL FTICR Predator Cell Controller. Sample solutions in THF at concentrations of approximately 1 x 10^{-4} M were continuously injected into source capillary of the mass spectrometer through a 30 μm needle (New Objective, Inc.) at a flow rate of 2.5 μL/min. Most importantly, the needle and capillary were isolated in a chamber to avoid oxidation by maintaining a slight overpressure of N_2. Nitrogen was also used as drying gas with a flow rate of 15.0 L/min at approximately 220 °C. The electrospray needle was typically held at 2.5 kV.

Synthesis of Na[L^{Me}Fe(μ-H)(μ-S)FeL^{Me}] (2). [L^{Me}FeH]$_2$ (50.2 mg, 0.0529 mmol) was dissolved in benzene (15 mL) to give a brown solution. The solution was transferred to a resealable flask and sodium dodecanethiolate (13.1 mg, 0.584 mmol) was added to the solution. A magnetic stir bar was added and the flask was sealed with a teflon pin. The mixture was warmed to 60 ˚C and stirred for 16 h, and the color of the solution changed to dark maroon. The solution was filtered, and volatile materials were removed under vacuum. The solid was redissolved in pentane (5 mL) and filtered. The volume was concentrated to 2 mL and the solution was cooled to -45˚ C overnight to yield dark red crystals. ^{1}H NMR (25 ˚C, C_6D_6): δ 24.3 (2H, βC*H*), 10.8 (12H, αCCH_3), -0.5 (28H, CHCH$_3$CH_3 and *p*-Ar), -2.9 (8H, C*H*CH$_3$CH$_3$), -4.3 (8H, *m*-Ar), -15.6 (24H, CHCH_3CH$_3$) ppm (Figure S-1). Further characterization was not pursued because of the impurities observed by ^{1}H NMR and Mossbauer spectroscopies. Synthesis of Na[L^{Me}Fe(μ-D)(μ-S)FeL^{Me}] (**2-D**) was performed in an analogous manner, using [L^{Me}FeD]$_2$ as starting material, and gave the same chemical shifts at 25 ˚C. The hydride/deuteride are not visible in the NMR spectrum because of their close proximity to the

paramagnetic metal center. Synthesis of Li[L^{Me}Fe(μ-H)(μ-S)FeL^{Me}] (**2-Li**) was performed in an analogous manner, using $LiSC_{12}H_{25}$ as starting material.

Synthesis of [NaCrypt-222][L^{Me}Fe(μ-H)(μ-S)FeL^{Me}] (3). 2.2.2-Cryptand (45.7 mg, 0.121 mmol) was dissolved in pentane (5 mL). Compound **2** (104.2 mg, 0.1040 mmol) was dissolved in pentane (5 mL) to give a dark maroon solution and was added dropwise to the cryptand solution, generating a purple precipitate. After settling for 1 h, the supernatant was decanted and discarded. The solid was dissolved in toluene (5 mL) and filtered. The filtrate was diluted with pentane (5 mL) and cooled to -40 ˚C overnight to yield dark crystals (78.3 mg, 54.6%). ^{1}H NMR (25 ˚C, THF-d_8): δ 7.3 (4H), 6.7 (8H), 4.4 (4H), 4.1 (12H, Cryptand), 4.0 (12H, Cryptand), 3.9 (4H), 3.1 (12H, Cryptand), 2.9 (2H), -1.5 (8H), -4.3 (8H) ppm (Figure S-2). ^{1}H NMR (THF-d_8, -80 ˚C): δ 10.1 (2H), 8.5 (2H), 6.8 (2H), 6.2 (4H), 5.4 (6H), 4.2 (30H), 3.3 (n/a), 2.4 (6H), 1.1 (18H), -0.6 / -0.7 (18H), -1.6 (8H), -2.0 (8H), -4.5 (2H), -5.1 / -5.3 (12H), -7.0 (2H), -16.0 (6H), -19.1 (2H), -23.7 (2H) ppm (Figure S-4 top). μ_{eff} (THF-d_8, 25 ˚C) = 3.06(8) μ_B. IR (cm^{-1}): 3050 (w), 2956 (m), 2919 (m), 2862 (m), 1516 (m), 1493 (m), 1458 (m), 1432 (m), 1396 (s), 1355 (m), 1313 (s), 1256 (m), 1233 (m), 1193 (w), 1171 (m), 1131 (m), 1100 (s), 1057 (m), 1039 (m), 1016 (m), 927 (m), 841 (w), 819 (w), 789 (m), 759 (m), 729 (s), 711 (w), 694 (m), 625 (w), 601 (w), 561 (w), 520 (m), 464 (m), 451 (m) (Figure S-12). UV-vis (THF; λ_{max}, nm (ε, $mM^{-1}cm^{-1}$)) 555 (3.72) (Figure S-15). Anal. Calcd for $C_{76}H_{119}N_6O_6NaSFe_2$•2($C_5H_{12}$): C, 67.78; H, 9.46; N, 5.52. Found: C, 67.86; H, 8.81; N, 5.58. [NaCrypt-222][L^{Me}Fe(μ-D)(μ-S)FeL^{Me}] (**3-D**) was synthesized analogously using **2-D** as starting material. Its ^{1}H NMR spectrum at -80 ˚C differed slightly (Figure S-4 bottom). [LiCrypt-222][L^{Me}Fe(μ-D)(μ-H)FeL^{Me}] (**3-Li**) was synthesized analogously using **2-Li** as starting material; its ^{1}H NMR spectrum is

shown at the bottom of Figure S-3 and the paramagnetically shifted peaks are identical to those of **3**.

Synthesis of [NaCrypt-222][L^{Me}Fe($CH_3C_6H_4CC$)(μ-S)FeL^{Me}] (4). Compound **3** (57.2 mg, 0.0415 mmol) was dissolved in THF (5 mL) to give a purple solution. A stock solution of 3-ethynyltoluene (0.53 mL of a 77 mM solution in THF, 0.041 mmol) was added to the solution of **3** via syringe and the mixture was shaken slightly. After 1 h the solution turned dark maroon. Volatile materials were removed under vacuum. The solid was washed with pentane (5 mL) and diethyl ether (5 mL). The solid was dissolved in THF (3 mL), filtered, and cooled to -40 ˚C to yield red crystals (32.9 mg, 53.8%). ^{1}H NMR (THF-d_8, 25 ˚C): δ 21.3, 8.3, 5.8, 4.0, 3.8, 3.0, 1.3, -0.4, -3.2 ppm (integrations not reported due to heavy overlap) (Figure S-5 bottom). ^{1}H NMR (THF-d_8, -80 ˚C): δ 17.7 (2H), 15.5 (3H), 10.2 (2H), 6.8, 4.5, 2.2, -0.7, -1.8, -2.3, -3.2, -3.5, -6.4 (6H), -19.4 (3H), -29.9 (2H) ppm (Figure S-5 top). μ_{eff} (THF-d_8, 25 ˚C) 4.4(2) μ_B. IR (cm^{-1}): 3051 (w), 2955 (m), 2918 (m), 2862 (m), 2821 (w), 1999 (m), 1790 (w), 1592 (w), 1572 (w), 1522 (m), 1460 (m), 1434 (m), 1404 (m), 1378 (m), 1355 (m), 1317 (m), 1300, (m), 1258 (m), 1231 (m), 1175 (m) 1132 (s), 1102 (s), 1088 (s), 1073 (m), 1036 (m), 1022 (m), 1004 (m), 938 (m), 926 (s), 841 (w), 820 (m), 792 (m), 781 (m), 760 (m), 743 (m), 709 (m), 693 (m), 636 (m), 583 (w), 560 (m), 520 (m), 446 (m) (Figure S-13). UV-vis (THF; λ_{max}, nm (ε, mM^{-1}cm^{-1})) 485 (6.10) (Figure S-16). Anal. Calcd for $C_{85}H_{125}N_6O_6NaSFe_2$•2($C_4H_8O$): C, 68.20; H, 8.68; N, 5.13. Found: C, 68.24; H, 8.65; N, 5.11.

Synthesis of [NaCrypt-222][L^{Me}Fe(μ-CHOO)(μ-S)FeL^{Me}] (5). On a Schlenk line, a volume bulb (60 mL) was was filled with CO_2 (28 mbar, 0.070 mmol). In an argon glovebox, **3** (38.9 mg, 0.0282 mmol) was dissolved in THF (3 mL) to give a purple solution that was transferred to a three-neck round bottom flask. The flask was fitted with the volume bulb, a

vacuum adapter, and a glass stopper. The vacuum tap was opened for 5 seconds, then closed. The volume bulb was opened to the flask. After 3 h, the solution turned dark red and crystals formed. The supernatant was decanted, and the crystals were washed with THF (2 mL) and dried under vacuum (30.0 mg, 74.7%). ^{1}H NMR (pyridine-d_5, 25 ˚C): δ 10.5 (1H, C*H*OO), 9.9 (4H), 9.3(4H), 4.6 (12H), 3.53 (12H, Cryptand), 3.47 (12H, Cryptand), 2.5 (12H, Cryptand), 0.29 (8H), -1.4 (12H), -2.7 (12H), -3.0 (8H), -14.1 (2H, βC*H*), -19.7 (12H) ppm (Figure S-6). μ_{eff} (pyridine-d_5, 25 ˚C) 4.1(3) μ_B. IR (cm^{-1}): 3053 (w), 2957 (m), 2920 (m), 1599 (m), 1521 (m), 1460 (m), 1434 (m), 1404 (s), 1355 (m), 1318 (m), 1261 (m), 1232 (w), 1175 (m), 1133 (m), 1103 (s), 1058 (m), 1037 (m), 1021 (m), 928 (m), 844 (w), 820 (w), 792 (m), 759 (m), 712 (w), 633 (w), 594 (w), 560 (w), 520 (w), 487 (w), 424 (w) (Figure S-14). UV-vis (THF; λ_{max}, nm (ε, mM^{-1}cm^{-1})) 527 (1.7), 438 (1.4) (Figure S-17). Anal. Calcd for $C_{77}H_{119}N_6O_8NaSFe_2$: C, 64.97; H, 8.43; N, 5.90. Found: C, 65.05; H, 8.59; N, 5.50.

Reduction of [NaCrypt-222][L^{Me}Fe(μ-H)(μ-S)FeL^{Me}] (3). Under an N_2 atmosphere, compound **3** (15.8 mg, 0.0115 mmol) was dissolved in THF (5 mL) and transferred onto KC_8 (3.8 mg, 0.028 mmol). The solution turned dark green and the reaction was stirred for 30 min. The solution was filtered, and volatile materials were removed under vacuum. The solid was redissolved in diethyl ether (2 mL), filtered, concentrated to 0.5 mL and cooled to -40 ˚C, yielding dark crystals. ^{1}H NMR spectroscopy indicated the presence of K_2[L^{Me}Fe(μ-S)FeL^{Me}] and K_2[L^{Me}Fe(μ-N_2)FeL^{Me}] with 1:3 relative integrations (Figure S-7). Both of these complexes have been characterized previously.[3,4]

Unsuccessful Alternate Syntheses of 2 and 3. Under N_2 atmosphere, sodium hydride (0.9 mg, 0.04 mmol) was weighed into a vial. L^{Me}Fe(μ-S)FeL^{Me} (32.0 mg, 0.0327 mmol), synthesized using published methods,[3] was weighed into a separate vial, dissolved in THF (~5

mL) and transferred to the sodium hydride. The reaction was stirred for 5 h. Examination of the product by ^{1}H NMR spectroscopy in C_6D_6 indicated little reaction occurring and no formation of **2** (Figure S-8).

Complex **1** (10.6 mg, 0.0112 mmol) was weighed into a vial, dissolved in C_6D_6, (0.4 mL) and transferred to a J. Young tube. Sodium triphenylmethanethiolate (3.3 mg, 0.011 mmol) was dissolved in C_6D_6 (0.3 mL) and transferred to the tube. After 48 hours, ^{1}H NMR spectroscopy indicated a large number of products with no clear indication of the formation of **2** (Figure S-9).

$L^{Me}Fe(\mu\text{-}S)FeL^{Me}$ (50.2 mg, 0.0513 mmol) was dissolved in THF (~5 mL) and stirred over a sodium mirror (15.9 mg, 0.692 mmol) for 1.5 hours, turning the solution dark green. The product was dried under vacuum, redissolved in pentane (~5 mL), filtered, reduced to ~ 2 mL, and stored in -40 ˚C. After 24 hours, dark green crystals formed. The ^{1}H NMR spectrum of these crystals in C_6D_6 (Figure S-10) is analogous to $K_2[^{Me}L^{Me}Fe(\mu\text{-}S)Fe^{Me}L^{Me}]$ and $Na_2[^{Me}L^{Me}Fe(\mu\text{-}S)Fe^{Me}L^{Me}]$ reported previously.[3] The crystalline product (12.6 mg) was dissolved in C_6D_6 (0.6 mL) and transferred to a J. Young tube, and then lutidinium chloride (1.9 mg, 0.013 mmol) was added. After 16 h of stirring, incomplete conversion to $L^{Me}Fe(\mu\text{-}S)FeL^{Me}$ is observed by ^{1}H NMR with no detectable amount of **2** (Figure S-10).

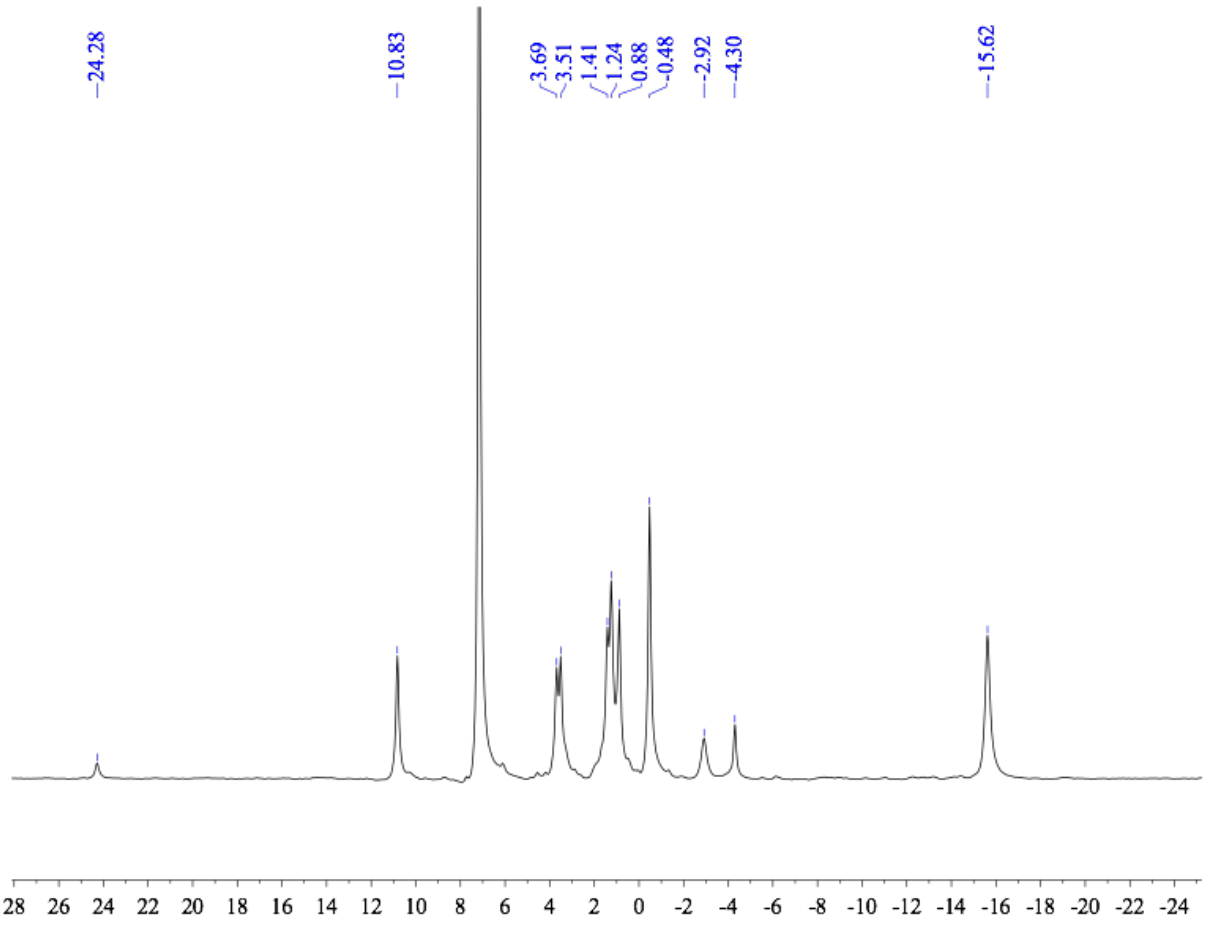

Figure S-1. ^{1}H NMR spectrum of Na[L^{Me}Fe(μ-H)(μ-S)FeL^{Me}] (**2**) in C_6D_6.

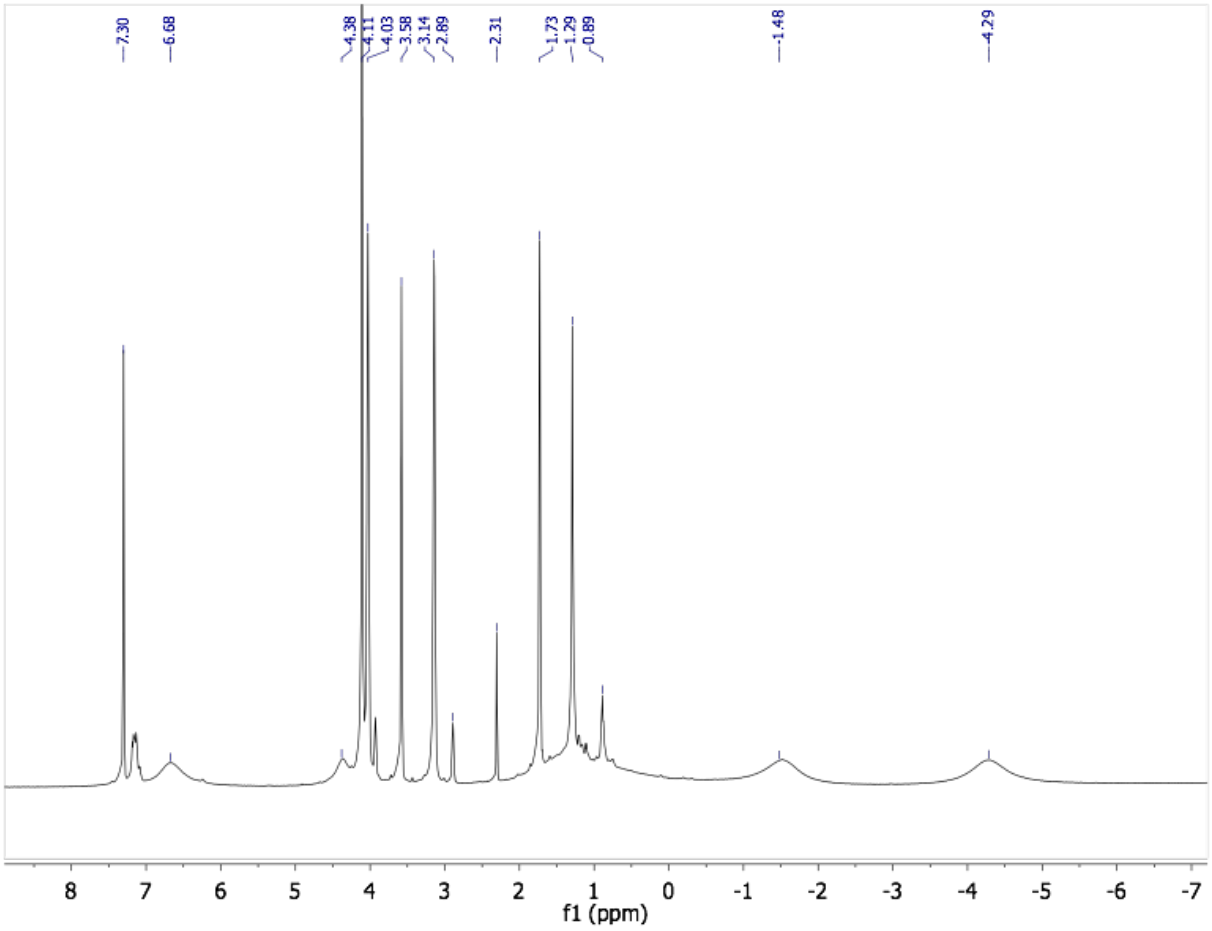

Figure S-2. ^{1}H NMR spectrum of [NaCrypt-222][L^{Me}Fe(μ-H)(μ-S)FeL^{Me}] (**3**) in THF-d_8, 25 ˚C.

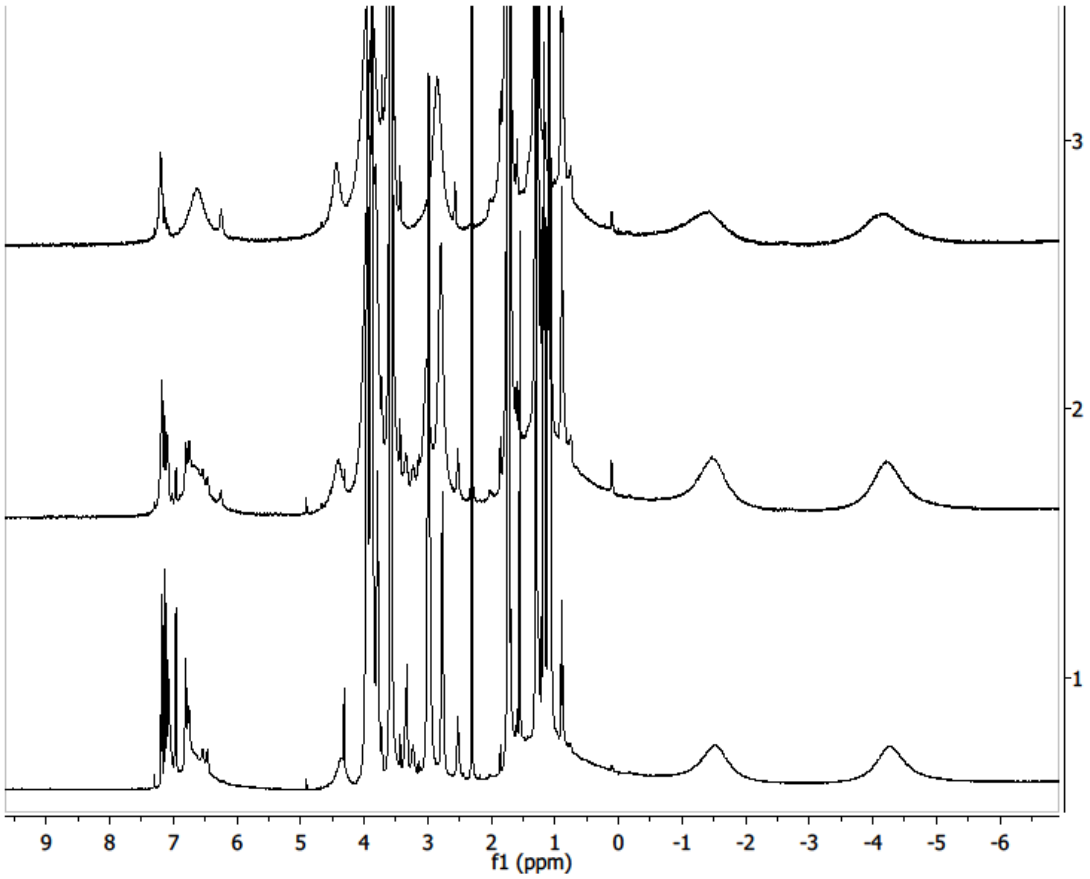

Figure S-3. ^{1}H NMR spectrum of [NaCrypt-222][L^{Me}Fe(μ-H)(μ-S)FeL^{Me}] (**3**) in THF-d_8, (top). A 1:1 mixture of [NaCrypt-222][L^{Me}Fe(μ-H)(μ-S)FeL^{Me}] (**3**) and [LiCrypt-222][L^{Me}Fe(μ-H)(μ-S)FeL^{Me}] (**3-Li**) (middle). A spectrum of [LiCrypt-222][L^{Me}Fe(μ-H)(μ-S)FeL^{Me}] (**3-Li**) in THF-d_8, (bottom).

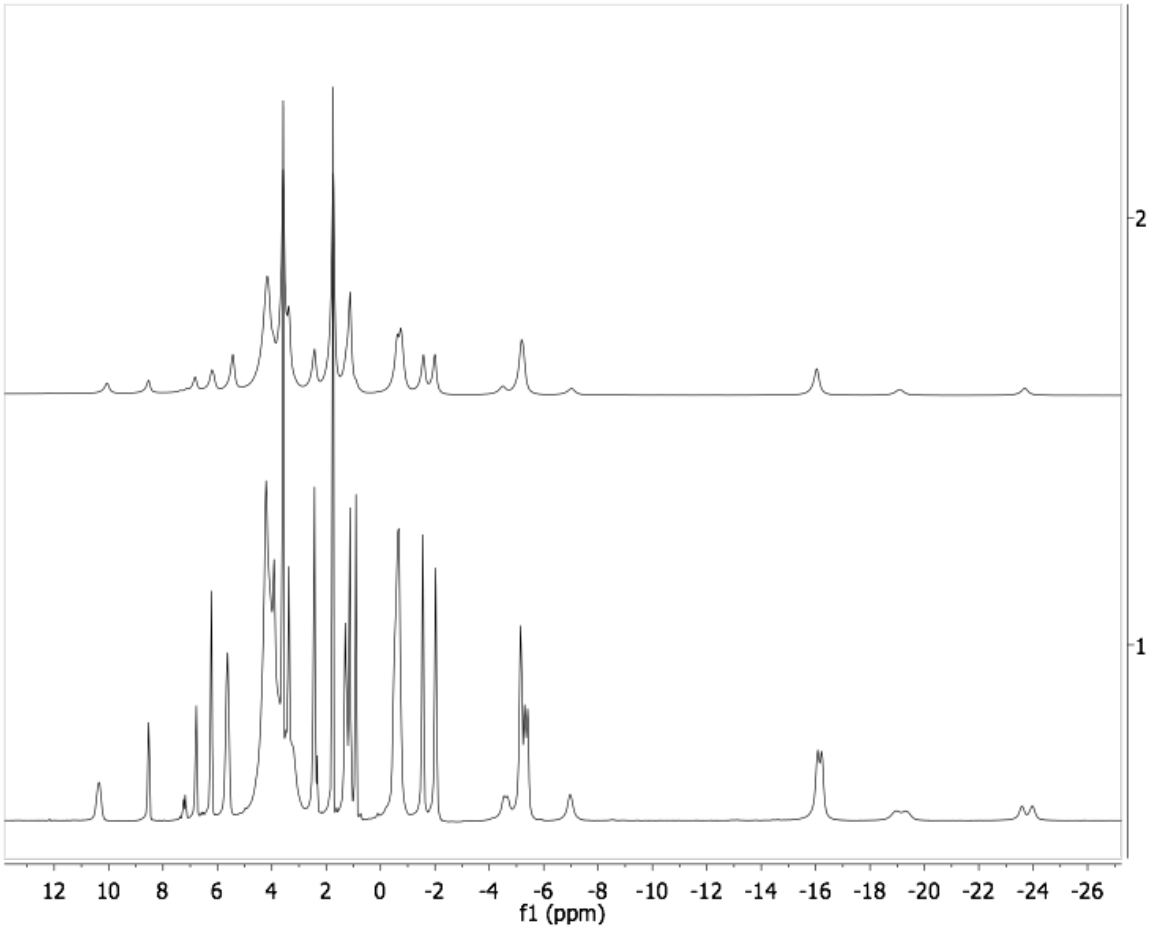

Figure S-4. ^{1}H NMR spectrum of [NaCrypt-222][L^{Me}Fe(μ-H)(μ-S)FeL^{Me}] (**3**) in THF-d_8, -80 ˚C (top). A 1:1 mixture of [NaCrypt-222][L^{Me}Fe(μ-H)(μ-S)FeL^{Me}] (**3**) and [NaCrypt-222][L^{Me}Fe(μ-D)(μ-S)FeL^{Me}] (**3-D**) at -80 ˚C (bottom).

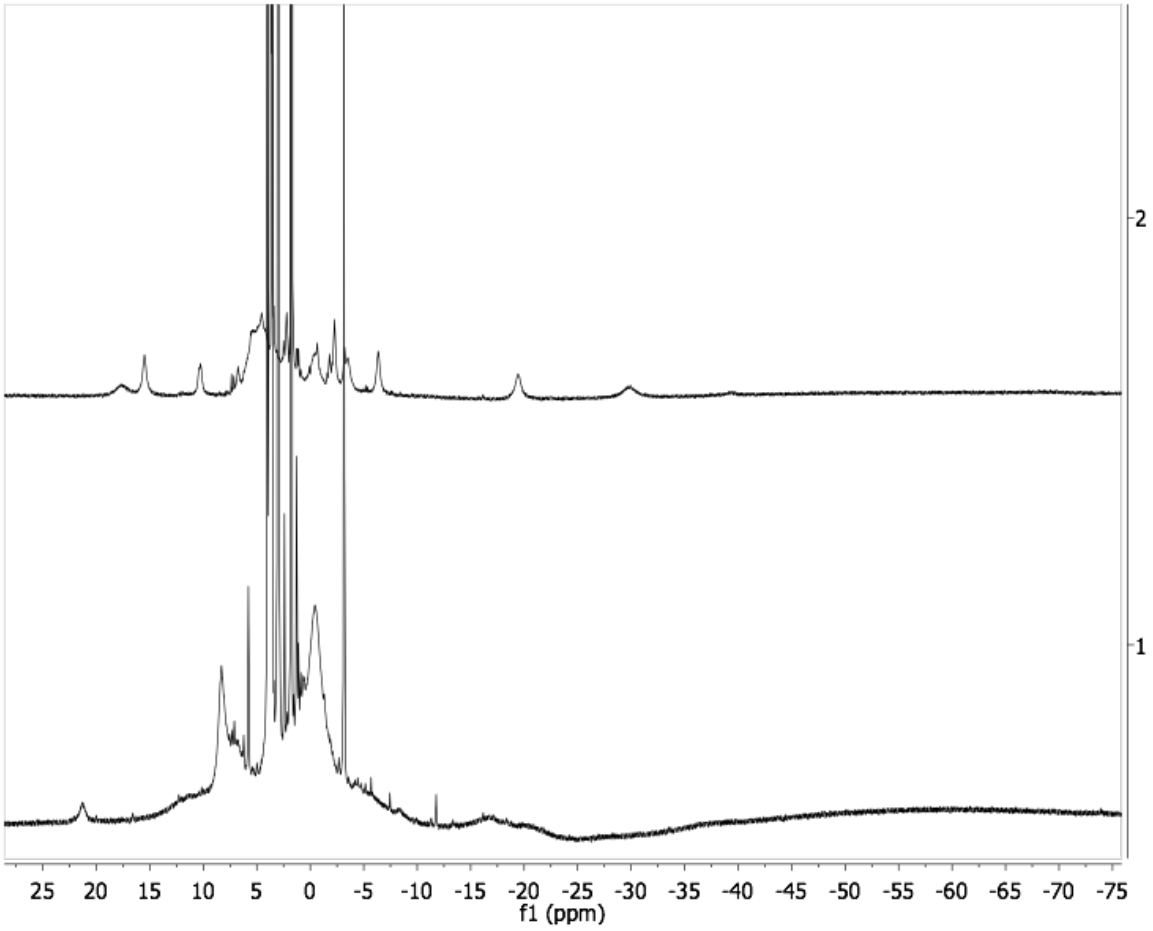

Figure S-5. ^{1}H NMR spectrum of [NaCrypt-222][$L^{Me}Fe(CH_3C_6H_4CC)(\mu$-S)Fe$L^{Me}$] (**4**) in THF-$d_8$, -80 ˚C (top), 25 ˚C (bottom).

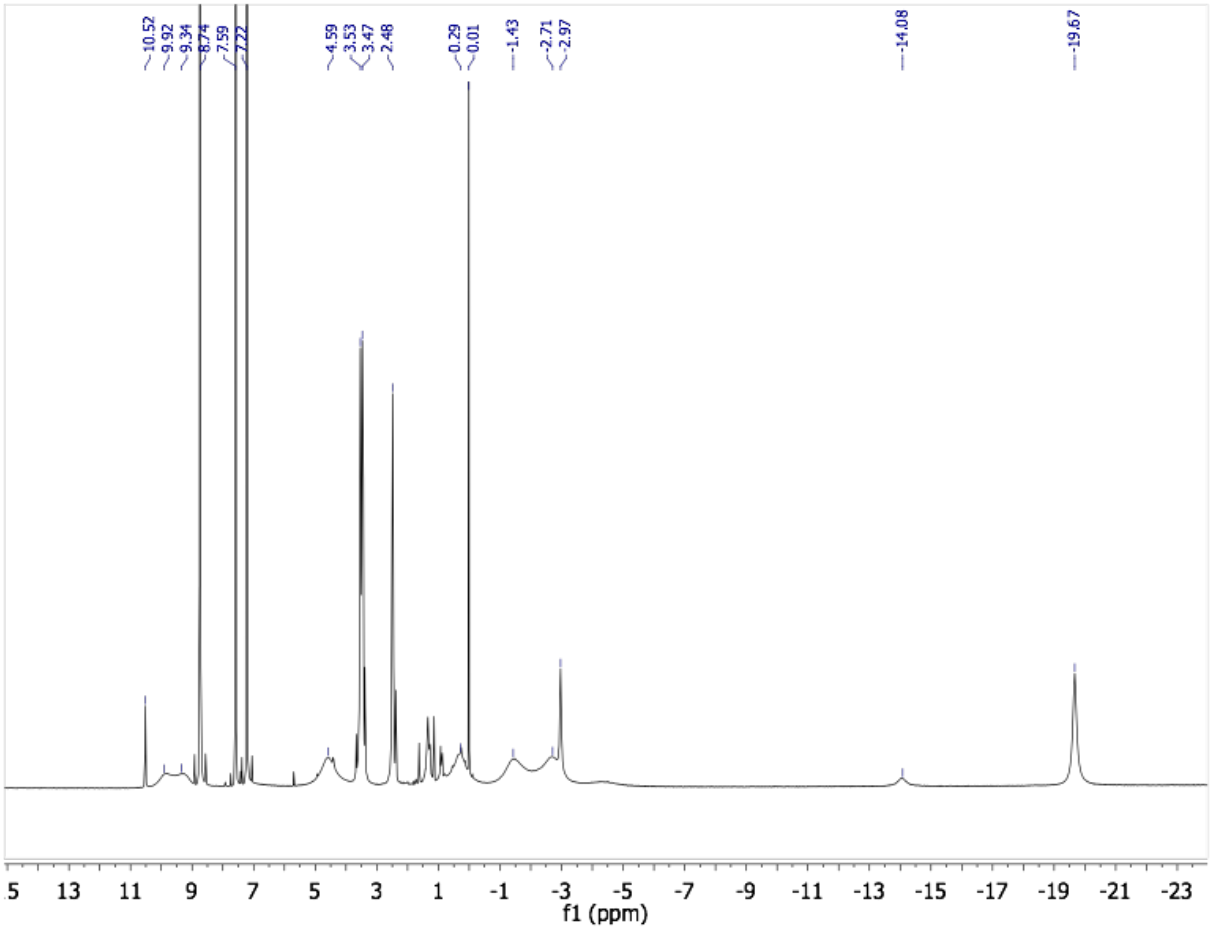

Figure S-6. ^{1}H NMR spectrum of [NaCrypt-222][L^{Me}Fe(CHOO)(μ-S)FeL^{Me}] (**5**) in pyridine-d_5.

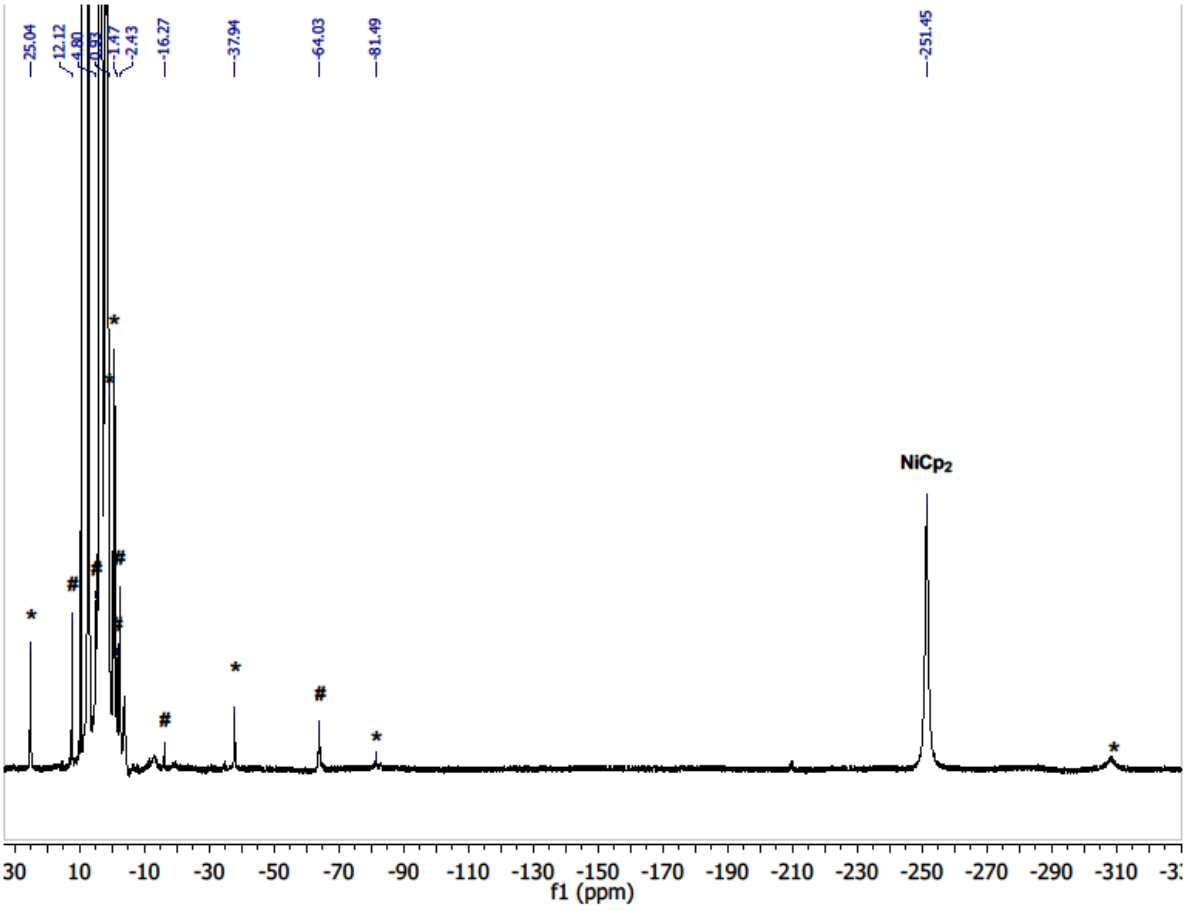

Figure S-7. ^{1}H-NMR spectrum of the reduction of **3** under N_2, benzene extract. Peaks marked with # correlate to $K_2[L^{Me}Fe(\mu\text{-}S)FeL^{Me}]$, and those marked with * correlate to $K_2[L^{Me}Fe(\mu\text{-}N_2)FeL^{Me}]$.[3,4]

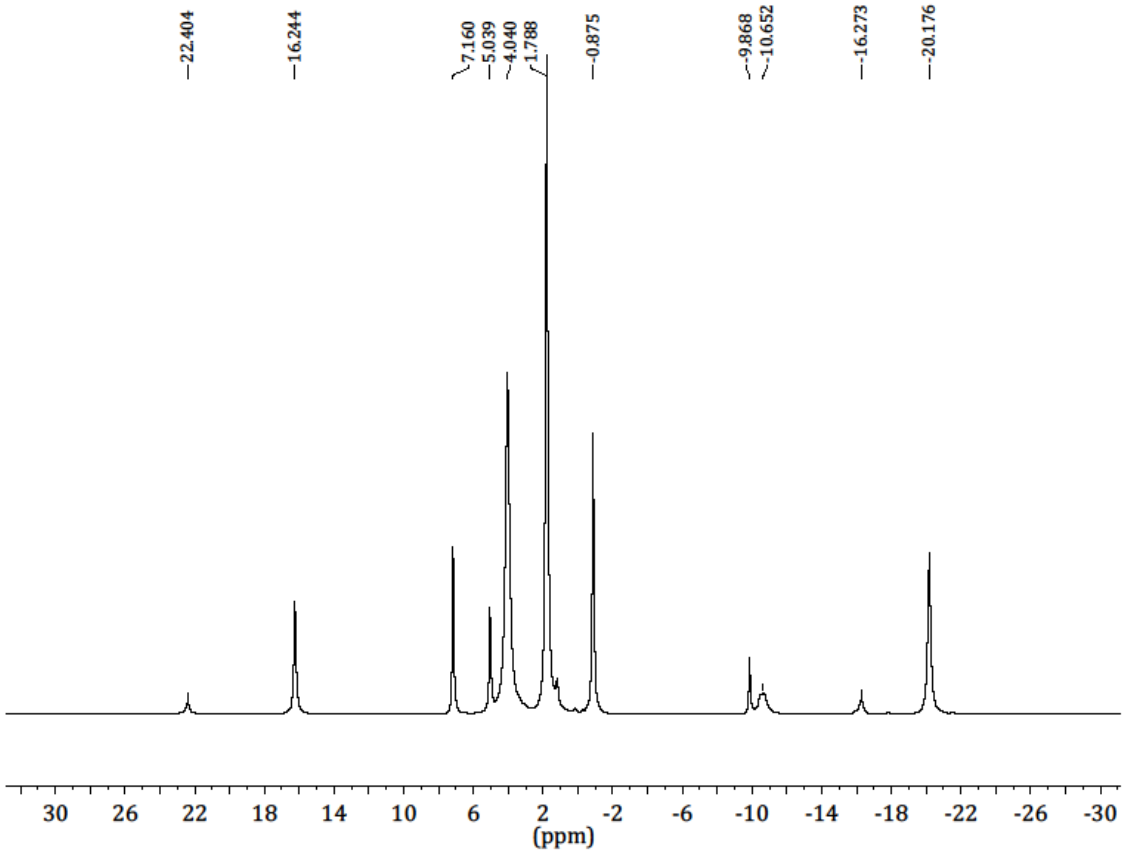

Figure S-8. ^{1}H NMR spectrum of $L^{Me}Fe(\mu\text{-}S)FeL^{Me}$ in C_6D_6 after stirring over NaH for 5 hours. The spectrum does not have any of the characteristic resonances of **2**.

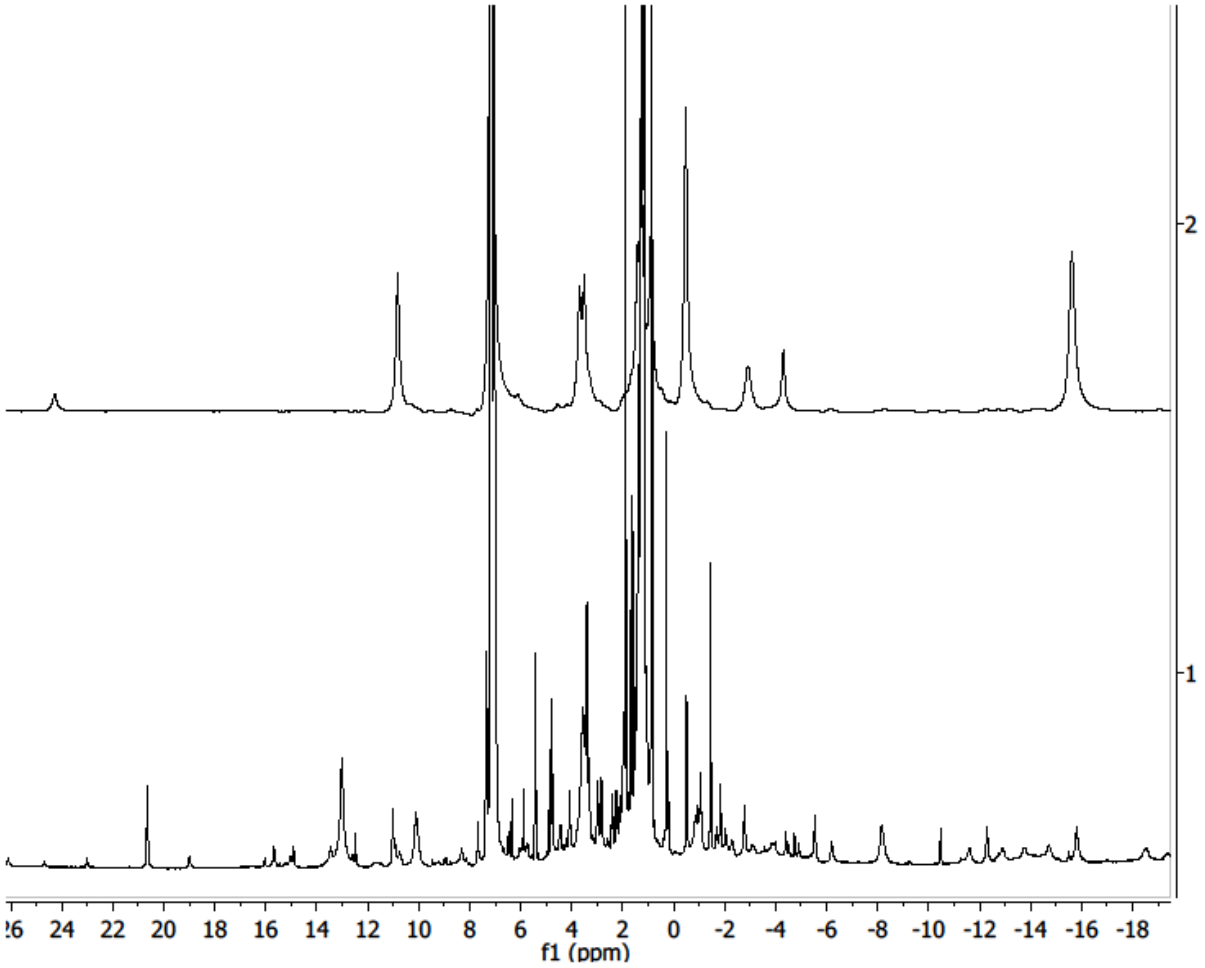

Figure S-9. A ^{1}H NMR spectrum of the reaction mixture from **1** and sodium triphenylmethanethiolate (bottom) and the clean spectrum of **2** (top).

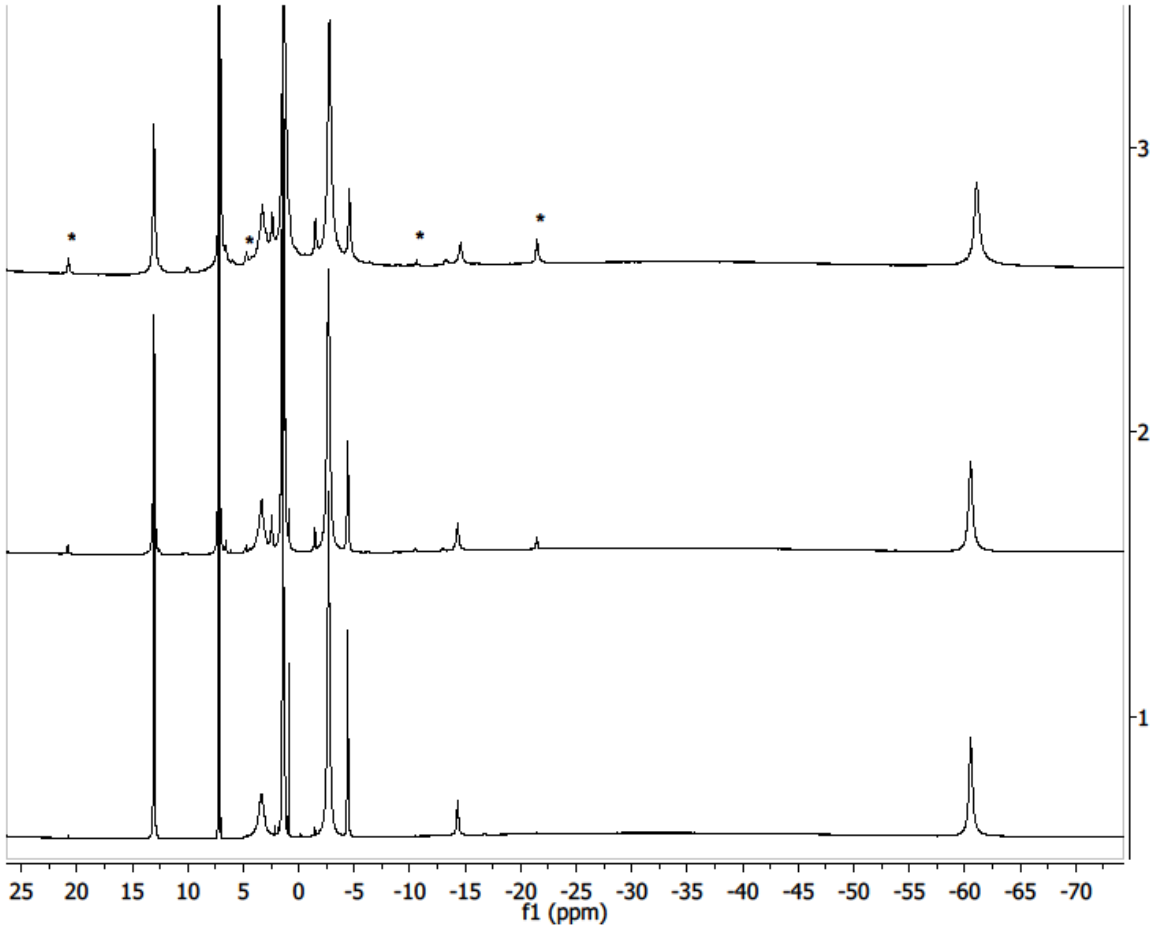

Figure S-10. ^{1}H NMR spectrum of $L^{Me}Fe(\mu\text{-}S)FeL^{Me}$ reduced with sodium metal (bottom). Spectrum 1 h after the addition of lutidinium chloride (middle). Spectrum 16 h after addition of lutidinium chloride (top). Peaks correlating to the $L^{Me}Fe(\mu\text{-}S)FeL^{Me}$ complex are marked with stars. The spectrum does not have any of the characteristic resonances of **2**.

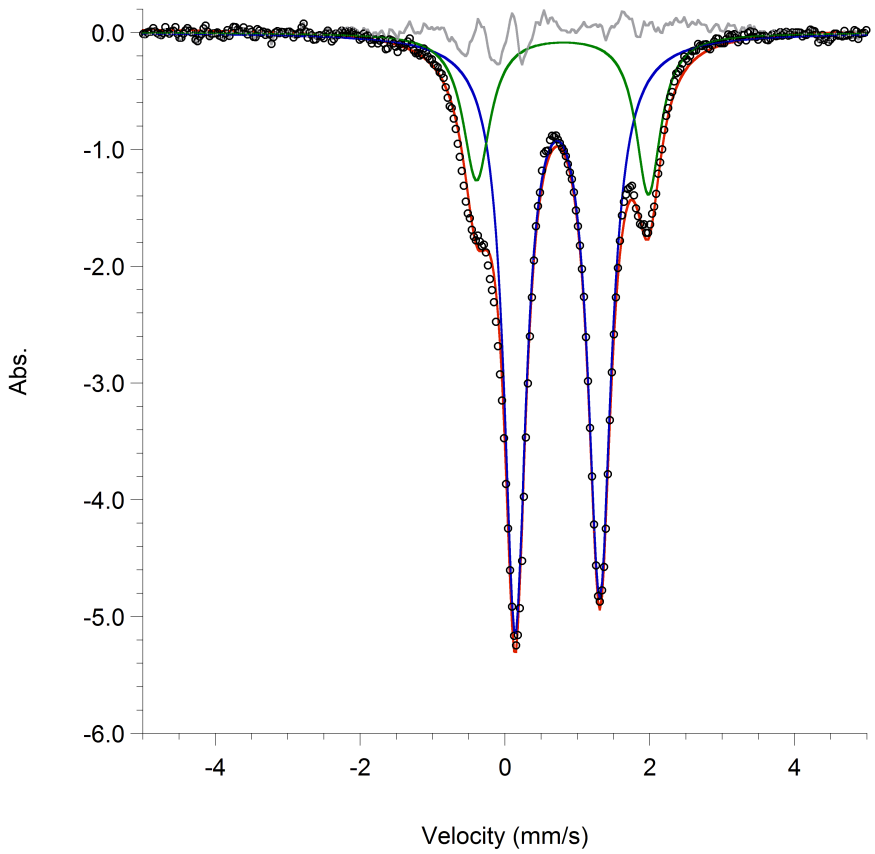

Figure S-11. Zero-field Mössbauer spectrum of the crude reaction mixture from the reaction of $[L^{Me}FeH]_2$ (**1**) with sodium dodecanethiolate (1 equiv). The spectrum was recorded on a solid sample at 80 K. The black dots are the data and the red line represents the sum of a major doublet for **2** (blue) and the $Na[L^{Me}Fe(SC_{12}H_{25})_2]$ byproduct (green). The major component (**2** in blue) has $\delta = 0.72$ mm/s and $|\Delta E_Q| = 1.16$ mm/s accounting for 77% of the sample. The minor component accounts for 23% of the sample with $\delta = 0.80$ mm/s and $|\Delta E_Q| = 2.38$ mm/s.

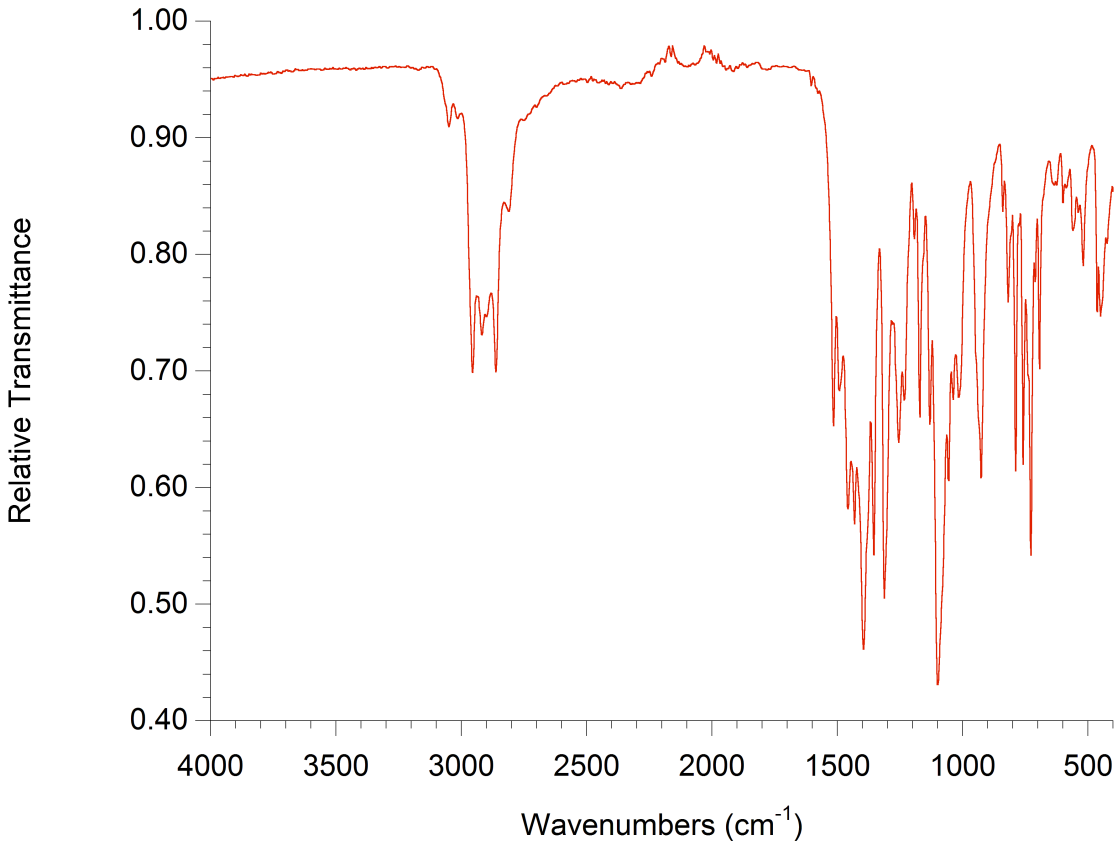

Figure S-12. IR spectrum of [NaCrypt-222][L^{Me}Fe(μ-H)(μ-S)L^{Me}] (**3**).

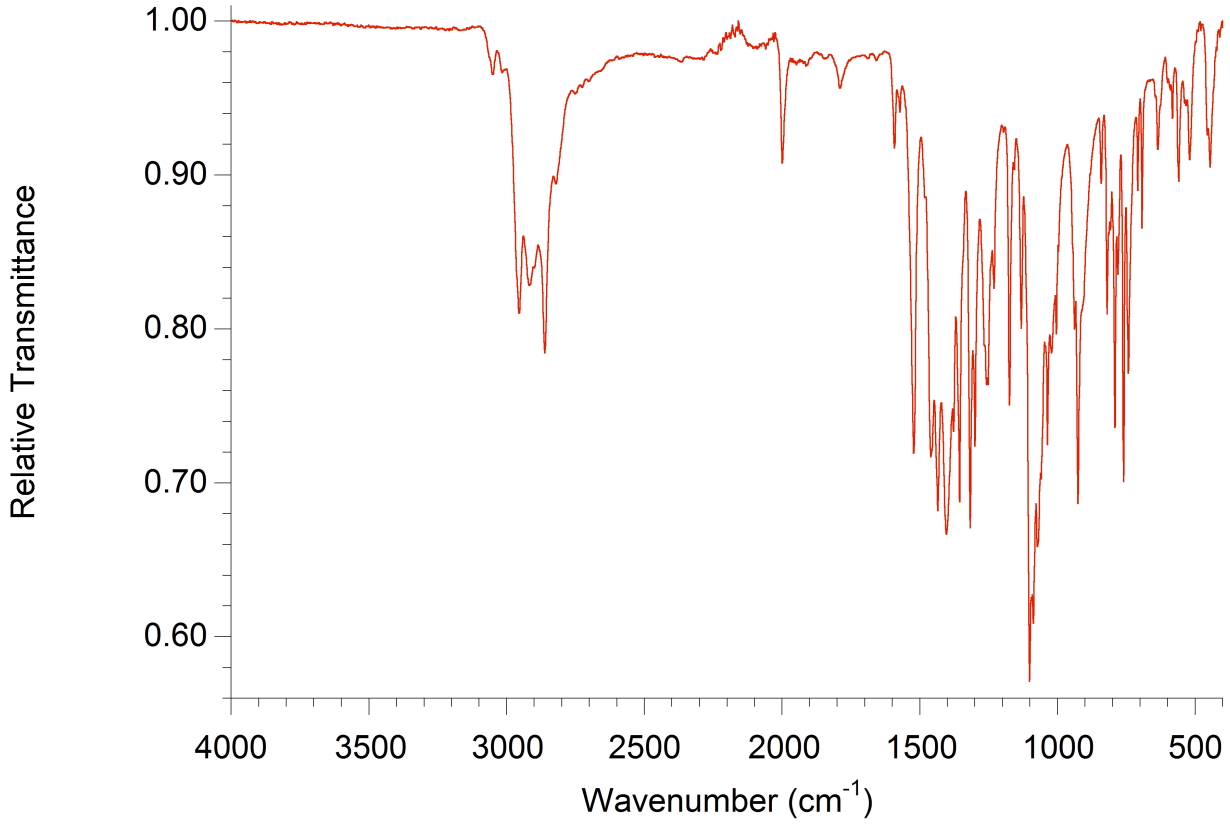

Figure S-13. IR spectrum of [NaCrypt-222][$L^{Me}Fe(CH_3C_6H_4CC)(\mu\text{-}S)FeL^{Me}$] (**4**).

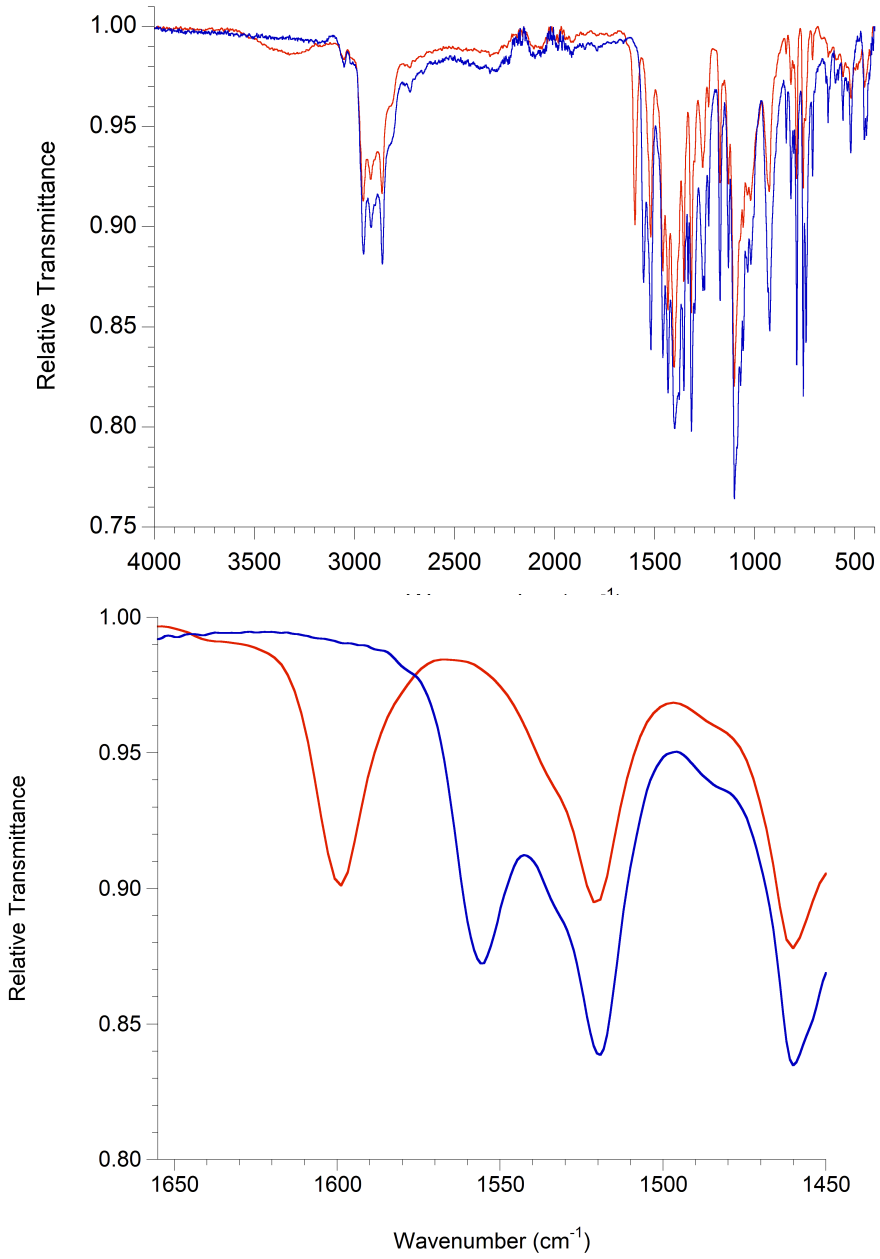

Figure S-14. IR spectra of [NaCrypt-222][L^{Me}Fe(μ-CHOO)(μ-S)FeL^{Me}] (**5**) synthesized with CO_2 (red) and with $^{13}CO_2$ (blue). The bottom spectrum is zoomed in to the region of interest for the C=O bands.

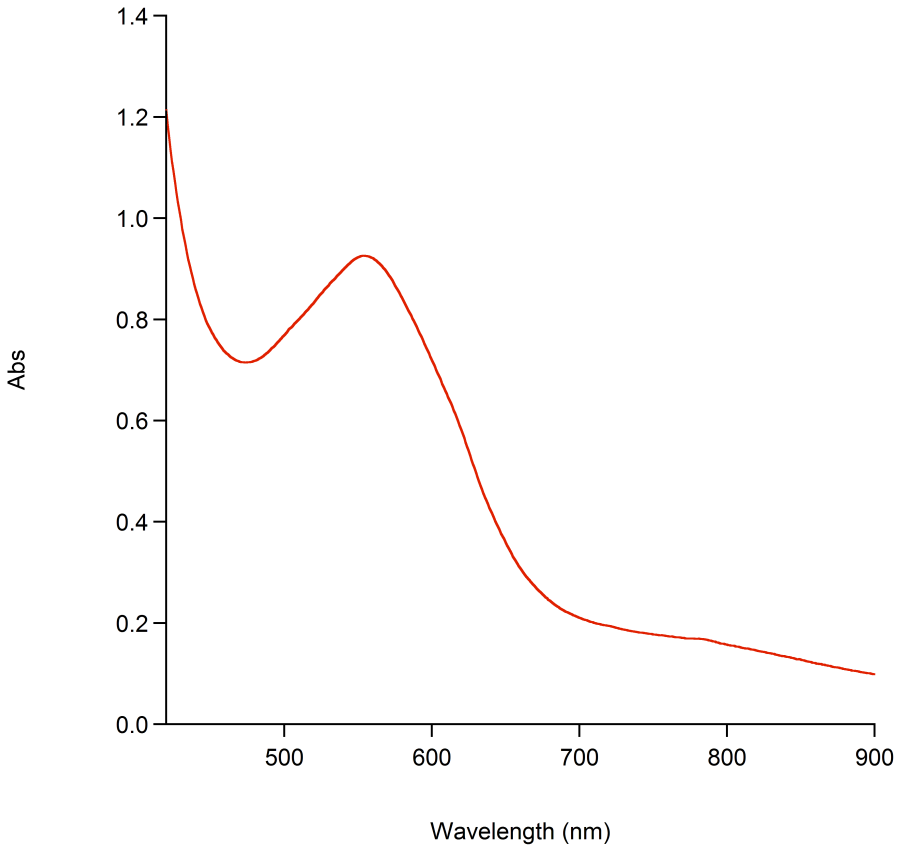

Figure S-15. UV-Vis spectrum of 0.26 mM [NaCrypt-222][L^{Me}Fe(μ-H)(μ-S)FeL^{Me}] (**3**) in THF through a 1 cm cell.

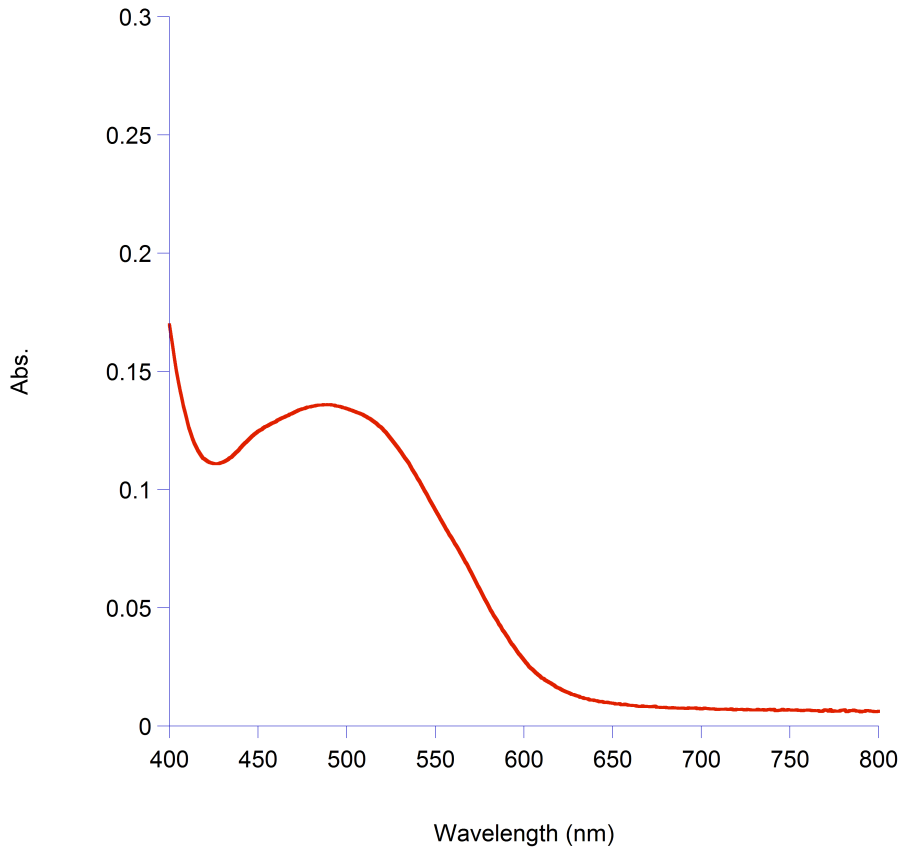

Figure S-16. UV-Vis spectrum of 0.20 mM [NaCrypt-222][$L^{Me}Fe(CH_3C_6H_4CC)(\mu\text{-}S)FeL^{Me}$] (**4**) in THF through a 1 mm cell.

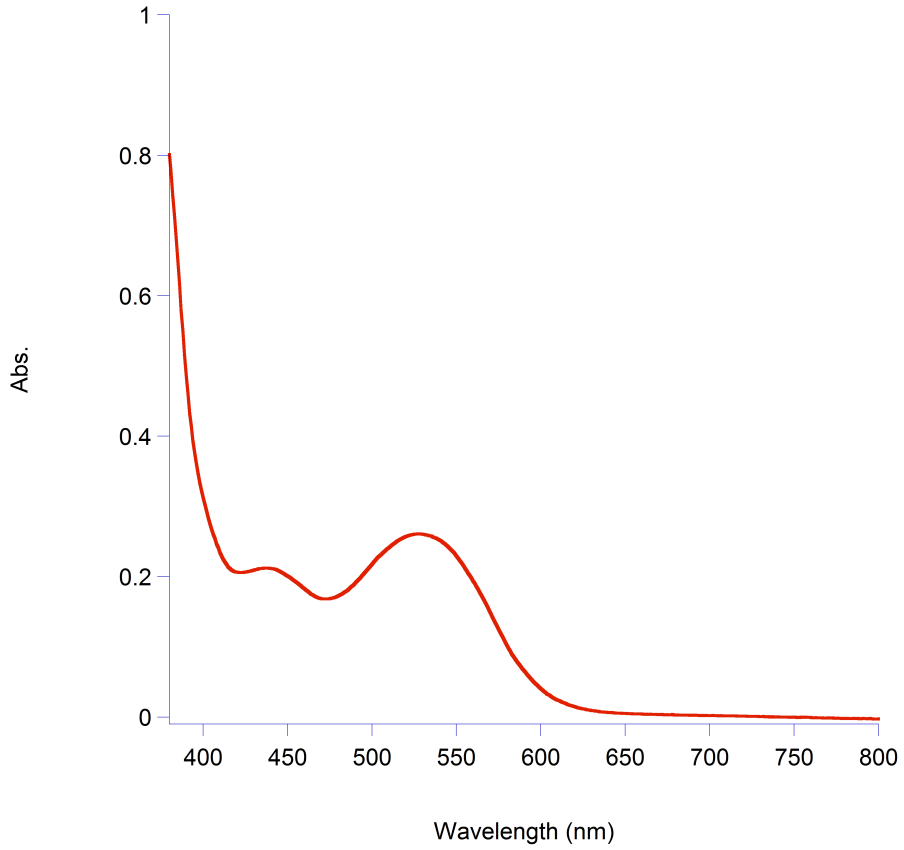

Figure S-17. UV-Vis spectrum of 0.14 mM [NaCrypt-222][L^{Me}Fe(CHOO)(μ-S)FeL^{Me}] (**5**) in THF through a 1 mm cell.

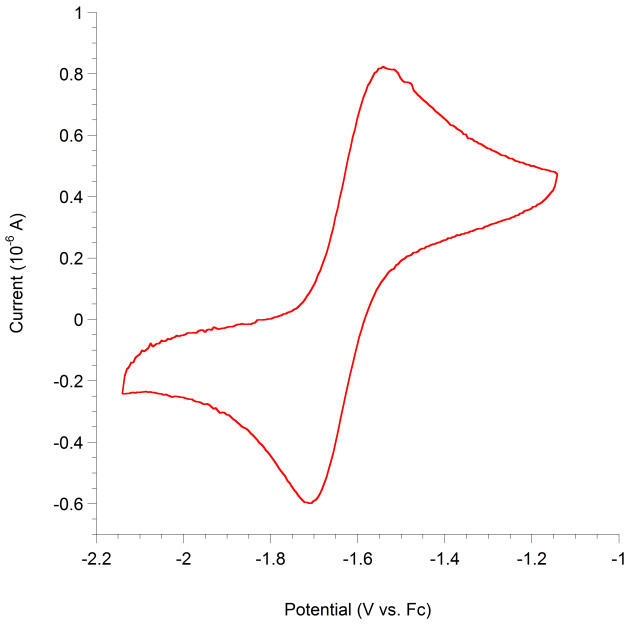

Figure S-18. Cyclic voltammogram of a 0.7 mM solution of [NaCrypt-222][L^{Me}Fe(μ-H)(μ-S)L^{Me}] (**3**) and 0.10 M tetrabutylammonium hexafluorophosphate in THF. A scan rate of 50 mV/s was used. The trace features a reversible oxidation at $E_{1/2}$ = -1.6 V vs. Fc.

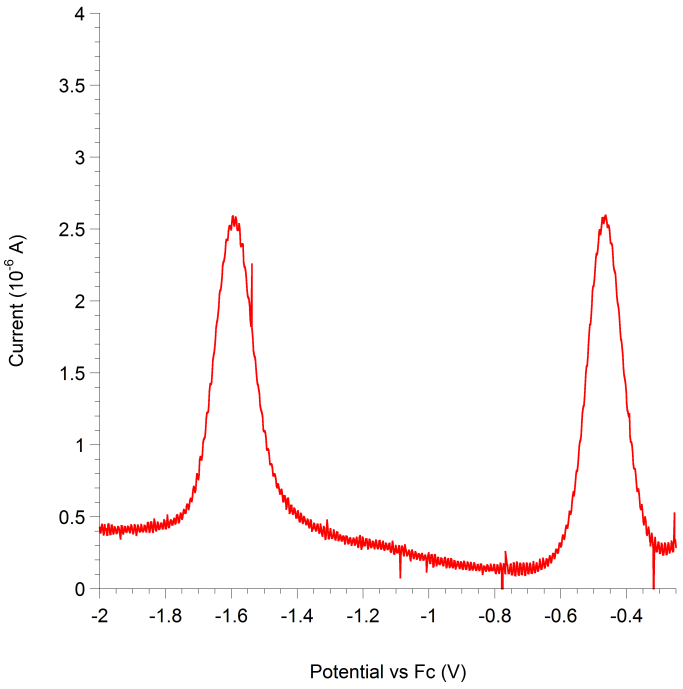

Figure S-19. A differential pulse voltammogram of **3** with 1.0 equiv of $FeCp^*_2$ as a concentration standard, using conditions described above. The similar peak sizes suggest that the oxidation of **3** at -1.6 V vs Fc is a single-electron oxidation.

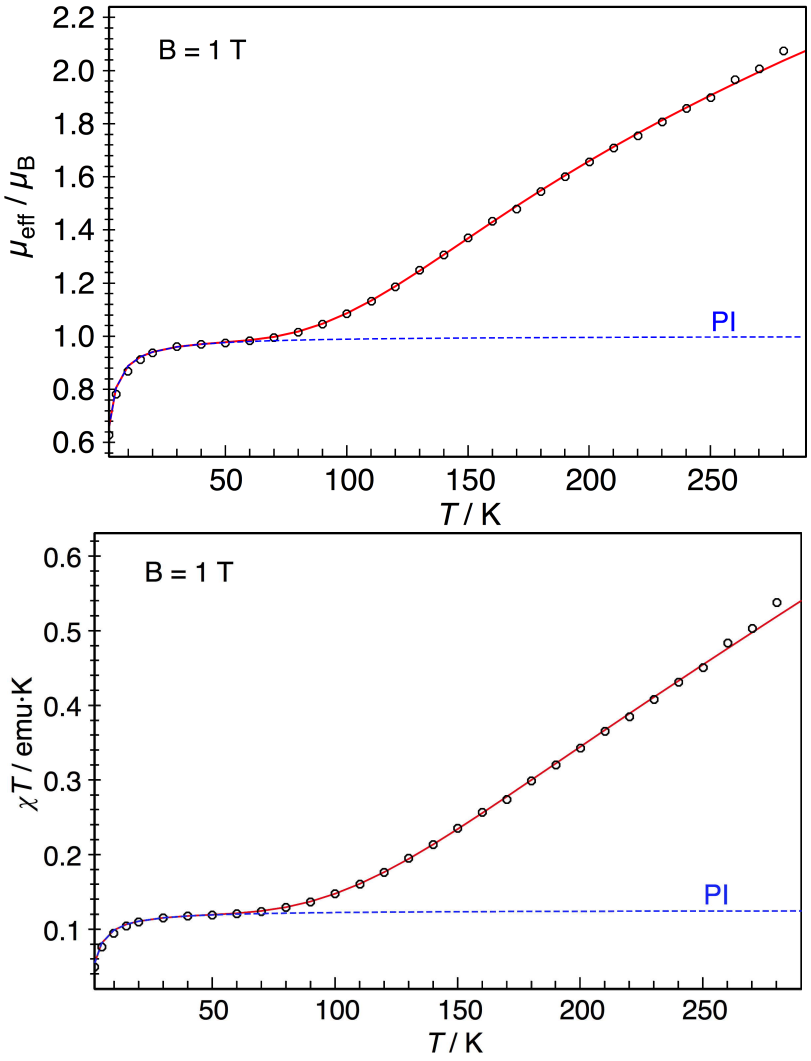

Figure S-20. Temperature dependence of the effective magnetic moment for a solid sample of **3**, viewed as effective magnetic moment and as χT. The red lines show a spin Hamiltonian simulation based on two $S_{Fe} = 2$ centers antiferromagnetically coupled with $J = -164$ cm^{-1} using the exchange Hamiltonian $H = -2J\mathbf{S}_1 \bullet \mathbf{S}_2$. The fit includes a component for a paramagnetic impurity (PI) of 4.2% of mononuclear iron(II) with $S = 2$. However, we cannot rule out the possibility that this impurity has a different spin.

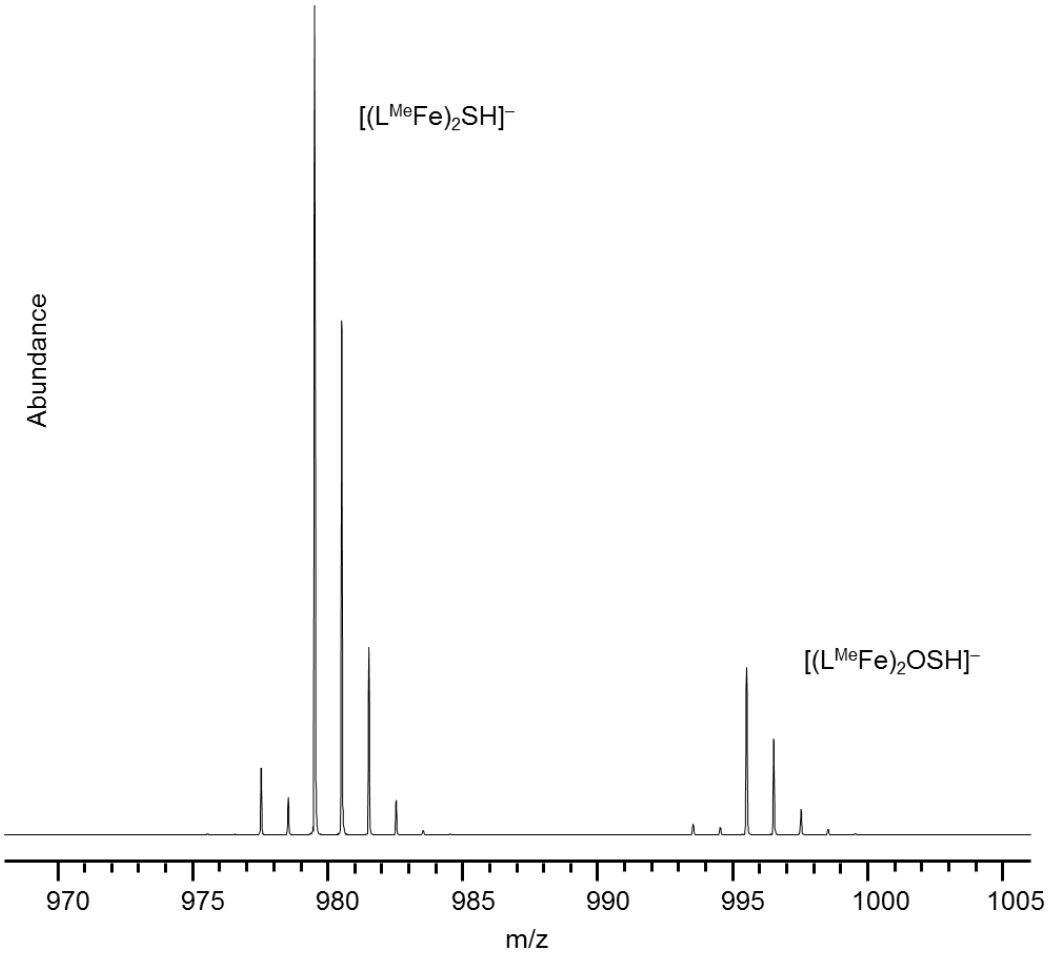

Figure S-21. ESMS data for **3**. The peaks on the left with a most abundant mass of *m/z* = 979.508 are consistent with the $[L^{Me}Fe(\mu\text{-}H)(\mu\text{-}S)FeL^{Me}]^-$ anion (predicted *m/z* = 979.504). A smaller contribution from an oxidized species was also detected consistent with composition $[(L^{Me}Fe)_2OSH]^-$ (right side of spectrum).

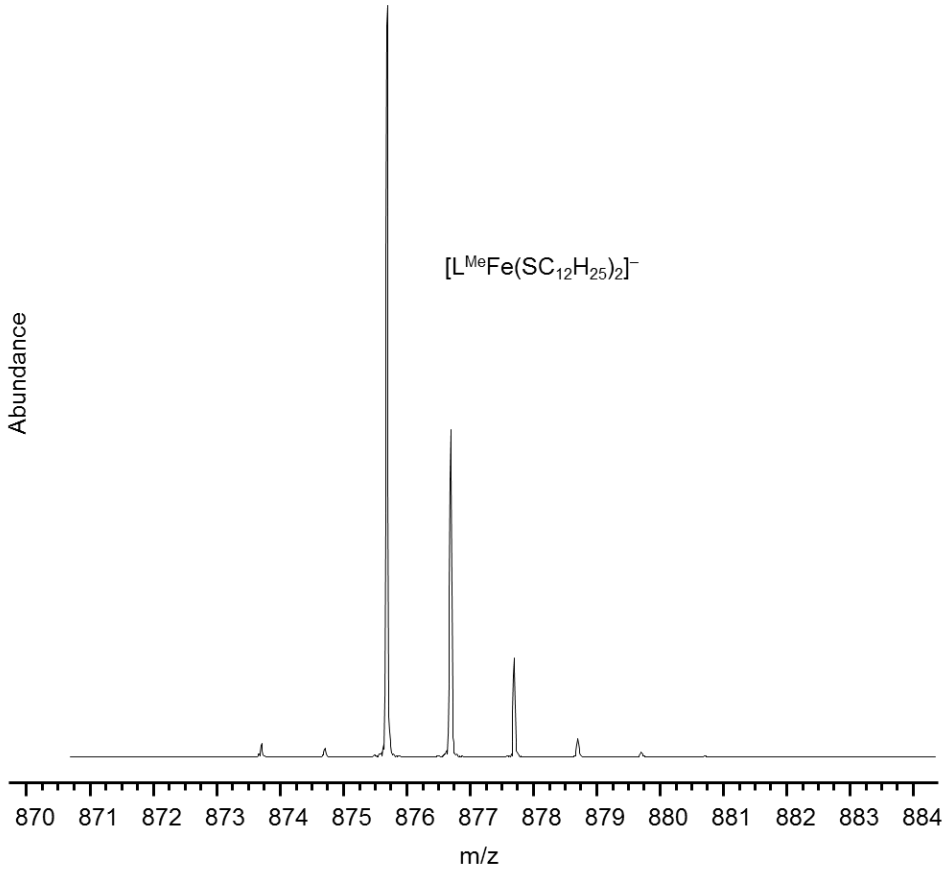

Figure S-22. ESMS data for minor component formed during the synthesis of **2**. The dominant isotopologue at mass of m/z = 875.582 and relative intensities are consistent with the $[L^{Me}Fe(SC_{12}H_{25})_2]^-$ anion (predicted *m/z* = 875.597).

X-ray Crystallography of 2 and 3. Crystals were placed on the tip of a 0.1 mm diameter glass capillary tube or fiber and mounted on a Bruker SMART APEX II CCD Platform diffractometer for a data collection at 100.0(1) K[5] using MoKα radiation and a graphite monochromator for the structures of **2** and **3**. A preliminary set of cell constraints and an orientation matrix were calculated from reflections harvested from three orthogonal wedges of reciprocal space. The intensity data were corrected for absorption.[6] The structures were solved using SIR97[7] and refined using SHELXL-97.[8] The space groups were determined based on systematic absences and intensity statistics. Direct-methods solutions were calculated, which provided most non-hydrogen atoms from the E-map. Full-matrix least-squares/difference Fourier cycles located the remaining non-hydrogen atoms. All non-hydrogen atoms were refined with anisotropic displacement parameters. All hydrogen atoms were placed in idealized positions and refined as riding atoms with relative isotropic displacement parameters, unless otherwise noted. Details of the crystal structures are presented in Table S-1.

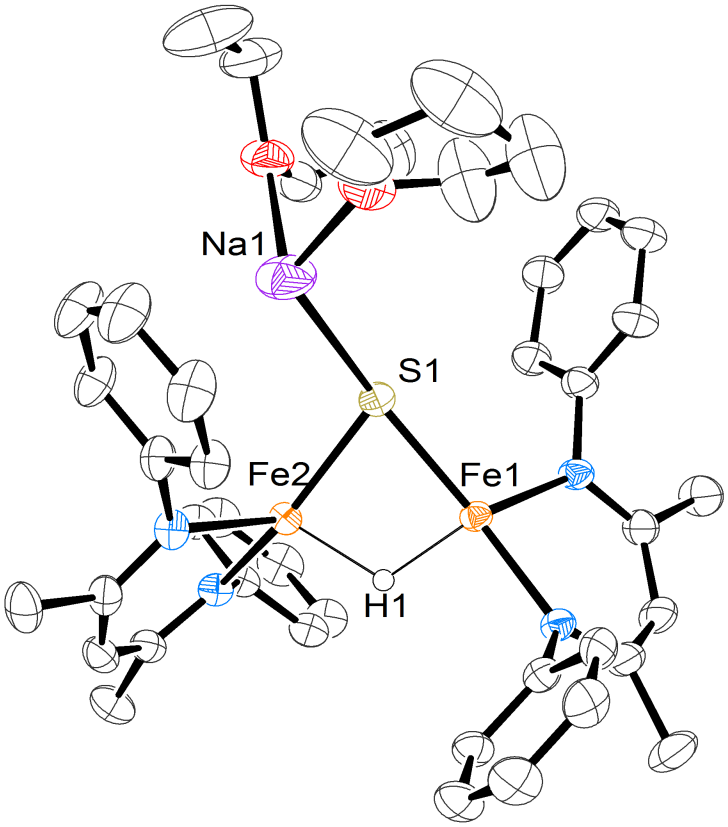

Figure S-23. Molecular structure of **2** with thermal ellipsoids shown at 50% probability. The hydrogen atoms, except for the hydride, and isopropyl groups of the aryl rings have been omitted for clarity.

X-ray Crystallography of 4 and 5. Low-temperature diffraction data (ω-scans) were collected on a Rigaku MicroMax-007HF diffractometer coupled to a Saturn994+ CCD detector with Cu Kα (λ = 1.54178 Å) for the structure of **4**. Low-temperature diffraction data (ω-scans) were collected on a Rigaku R-AXIS RAPID diffractometer coupled to an R-AXIS RAPID imaging plate detector with Mo Kα radiation (λ = 0.71073 Å) for the structure of **5**. All structures were solved by direct methods using SHELXS and were refined against F^2 on all data by full-matrix least squares with SHELXL.[8] All non-hydrogen atoms were refined anisotropically unless otherwise noted. Hydrogen atoms were included in the model at geometrically calculated positions and refined using a riding model unless otherwise noted. The isotropic displacement parameters of all hydrogen atoms were fixed to 1.2 time the *U* value of the atoms to which they are linked (1.5 times for methyl groups). All disorder was refined with similarity restraints on the 1,2- and 1,3- distances and displacement parameters.

Table S-1. Details of X-ray crystal structures.

Compound	Na[LMeFe(μ-H)(μ-S)FeLMe] **(2)**	[NaCrypt-222][LMeFe(μ-H)(μ-S)FeLMe] **(3)**	[NaCrypt-222][LMeFe($CH_3C_6H_4CC$)(μ-S)FeLMe] **(4)**	[NaCrypt-222][LMeFe(μ-CHOO)(μ-S)FeLMe] **(5)**
Empirical formula	$C_{70}H_{111}Fe_2N_4NaO_3S$	$C_{84}H_{139}Fe_2N_6NaO_8S$	$C_{93}H_{141}Fe_2N_6NaO_8S$	$C_{77}H_{119}Fe_2N_6NaO_8S$
FW	1223.38	1527.75	1637.86	1423.52
Crystal system	Monoclinic	Triclinic	Triclinic	Triclinic
Wavelength (Å)	0.71075	0.71075	1.54187	0.71075
Space group	*C* 2/*c*	*P*-1	*P*-1	*P*-1
a (Å)	47.214(7)	13.876(2)	13.2765(7)	12.7769(3)
b (Å)	12.720(2)	15.610(3)	17.673(1)	13.0700(3)
c (Å)	23.732(4)	20.119(3)	19.260(1)	13.577(1)
α (deg)	90	87.134(3)	94.225(7)	104.326(7)
β (deg)	102.646(2)	87.195(3)	94.850(7)	110.612(8)
γ (deg)	90	76.886(3)	95.622(7)	94.734(7)
V ($Å^3$)	13907(4)	4235(1)	4466.0(5)	2020.0(2)
Z	8	2	2	1
ρ (g/cm^3)	1.169	1.198	1.218	1.170
Wavelength (Å)	0.71075	0.71075	1.54187	0.71075
μ (mm^{-1})	0.499	0.428	3.315	0.444
*R*1, w*R*2 (I > 2σ(I))	0.0588, 0.1477	0.0690, 0.1471	0.0811, 0.1174	0.0905, 0.2281
*R*1, w*R*2 (all data)	0.0994, 0.1695	0.1345, 0.1730	0.2229, 0.1575	0.0999, 0.2329
GOF	1.046	1.032	0.890	1.151

References

[1] Dugan, T. R.; Bill, E.; MacLeod, K. C.; Brennessel, W. W.; Holland, P. L. *Inorg. Chem*. **2014**, *53*, 2370.

[2] Schubert, E. M. *J. Chem. Educ*. **1992**, *69*, 62.

[3] Rodriguez, M. M.; Stubbert, B. D.; Scarborough, C. C.; Brennessel, W. W.; Bill, E.; Holland, P. L. *Angew. Chem. Int. Ed*. **2012**, *51*, 8247.

[4] Smith, J. M.; Sadique, A. R.; Cundari, T. R.; Rodgers, K. R.; Lukat-Rodgers, G.; Lachicotte, R. J.; Flaschenriem, C. J.; Vela, J.; Holland, P. L. *J. Am. Chem. Soc*. **2006**, *128*, 756

[5] *APEX2*, version 2012.4-3; Bruker AXS: Madison, WI, 2012

[6] Sheldrick, G. M. *SADABS*, version 2008/1; University of Göttingen: Göttingen, Germany, 2008.

[7] Altomare, A.; Burla, M. C.; Camalli, M.; Cascarano, G. L.; Giacovazzo, C.; Guagliardi, A.; Moliterni, A. G. G.; Polidori, G.; Spagna, R. *SIR97: A new program for solving and refining crystal structures*; Istituto di Cristallografia, CNR: Bari, Italy, 1999.

[8] Sheldrick, G. M. *Acta Crystallogr*. **2008**, *A64*, 112.